University of Groningen

In-situ TEM analysis of the reduction of nanometre-sized Mn3O4 precipitates in a metal matrix
Kooi, B.J.; de Hosson, J.T.M.

Publication date:
2001

Link to publication in University of Groningen/UMCG research database

IN-SITU TEM ANALYSIS OF THE REDUCTION OF NANOMETRE-SIZED Mn₃O₄ PRECIPITATES IN A METAL MATRIX

B. J. KOOI and J. Th. M. DE HOSSON†

Laboratory of Applied Physics, Materials Science Centre and the Netherlands Institute for Metals Research, University of Groningen, Nijenborgh 4, 9747 AG Groningen, The Netherlands

Abstract—The objective of the present work is the in-situ study of the transformation of small oxide precipitates in a metal matrix by conventional and high-resolution transmission electron microscopy (HRTEM). As an example the reduction of Mn_3O_4 into MnO for nano-sized oxide precipitates in a silver matrix was studied in detail. A convenient method for monitoring the reduction process is shown for a large number of precipitates simultaneously. It is based on two-beam dark-field images showing distinct Moiré patterns for the MnO and the various types of Mn_3O_4 precipitates embedded within an Ag matrix. A controlling factor of the transformation kinetics appeared to be the rate in which the system can relax the strains due to the accompanying volume reduction of the precipitates. Other interesting aspects of the Mn_3O_4 to MnO transformation scrutinized and explained were the shape change of the precipitates upon reduction and the fact that mixed Mn_3O_4/MnO precipitates were only detected within a small temperature/time interval. Ostwald ripening of the MnO precipitates was observed as well. © 2001 Acta Materialia Inc. Published by Elsevier Science Ltd. All rights reserved.

Keywords: Transmission electron microscopy (TEM); Phase transformations; Composites; Kinetics; Interface

1. INTRODUCTION

The equilibrium phase of nano-sized particles may deviate from that of the bulk owing to the contributions of the surface energy and surface stress. For small inclusions also of the strain energy exerted by the matrix may become appreciable, in addition to the contribution of the interfacial energy. Striking examples of the effect of residual strain is the occurrence of "magic" sizes for Pb inclusions in an Al matrix [1] and the presence of solid noble gas inclusions at temperatures substantially above the triple point of these gases [2, 3]. Another example showing the strong influence of interfacial and strain energy on small inclusions can be found in the more classical precipitation sequence(s) in Al alloys e.g. GP zones, θ'', θ' and θ [4]. Knowledge and understanding of the behaviour of small particles and inclusions is of importance for many engineering materials, particularly with the ongoing trends towards materials with a controlled nano-structure. In

this context the study of phase transitions of small particles and inclusions deserves special attention, since it will probably play a key role in the improvement of the understanding and in the control of the microstructure.

Transmission electron microscopy (TEM) is particularly suited for in-situ studies of phase transitions of small particles and inclusions. Melting/solidification of particles and inclusions have particularly experienced considerable attention, e.g. [5–14]. Nevertheless, in-situ TEM studies of solid-state structural phase transformations in particles and inclusions have received only little systematic attention, an exception of which is the study of the transition from tetragonal to monoclinic ZrO_2 for small inclusions [15–20] motivated by technological applications [21–24] and the α to β transition in quartz [25, 26, 25, 26]. These transformations mentioned have a displacive character. To the best of our knowledge in-situ TEM studies of the transformation of oxide precipitates with changing composition, i.e. changing valence of the cations were not reported in the literature. Indeed some papers deal with the possibility of local reduction of bulk oxides by electron beam irradiation [27]. In this paper a detailed in-situ TEM study is presented of the reduction of small

---

† To whom all correspondence should be addressed. Tel.: +31-50-363-4898; Fax: +31-50-363-4881.

E-mail address: hossonj@phys.rug.nl (J.Th.M. De Hosson)

oxide precipitates, namely the Mn_3O_4 to MnO transformation for precipitates in an Ag matrix. For details of our previous work on these systems reference is made to [28–33]. This paper concentrates on (i) the demonstration of a convenient method based on Moiré patterns to follow the reduction for a large number of precipitates simultaneously, (ii) a quantitative determination of the reduction kinetics, (iii) an explanation of the observed transformation kinetics, (iv) an explanation of the observed shape change of the precipitates (v) an explanation of the observed Mn_3O_4/MnO interface within the precipitates during transformation and (vi) the demonstration of Ostwald ripening of transformed MnO precipitates.

2. EXPERIMENTAL

An alloy of silver containing 3 at% manganese was made in a high-frequency furnace by melting together the pure constituents (purity 99.99% by weight) in an alumina crucible under oxygen-free argon protective atmosphere. The ingot was homogenized (1 week 700°C in an evacuated quartz tube) and subsequently cold rolled from 4 mm down to 0.3 mm. Oxidation was performed in air at 900°C for 1 h. Subsequently, the samples were annealed in evacuated quartz tubes at 650°C for one week to allow equilibration to occur and for removing strains within the sample. An alloy of Pd containing 3 at.% Mn was made in an arc-furnace from high-purity (4N) base metals. The button was homogenized for 5 days at 850°C and slices with a thickness of 5 mm were cold-rolled down to 0.3 mm. Oxidation was performed in air at 1000°C for 2 days.

TEM samples were prepared by grinding, dimpling and ion milling 3 mm discs to electron transparency. For the in-situ TEM analysis of the reduction of Mn_3O_4 precipitates into MnO, a JEOL 2010F (2025 objective lens pole piece) was used with a double-tilt Gatan heating holder model 652. In the heating holder, on top of the furnace first a 100 μm Ta ring (2 mm inner and 3 mm outer diameter) is placed followed by the sample and with a 100 μm Ti ring (1.5 mm inner and 3 mm outer diameter) on top. The Ti ring is used as oxygen getter enabling the reduction process to be activated. The Mn_3O_4 to MnO reduction was followed isothermally at 400, 500, 600 and 700°C nominal temperature of the furnace in the heating holder. For increasing temperature, the temperature of the thin edges of the sample starts to deviate increasingly from the nominal temperature of the furnace. Two-beam bright and dark field images of the same area of the sample were recorded after fixed time intervals at the temperatures mentioned, followed by cooling to room temperature and waiting for some time, e.g. 10 min to allow the drift of the sample to become small enough. So heating/cooling cycles were used to follow the reduction process. The heating time at a certain temperature includes the time in which the temperature is raised from room tem-

perature to this certain temperature. In about 1 min the temperature is raised to about 30–40°C below the final temperature of 400–700°C. In the next minute the temperature difference with the nominal final temperature becomes less than about 3°C and approaches this final temperature smoothly without any overshoot. Besides the in-situ analysis in a JEOL 2010F, also a JEOL 4000 EX/II with a top-entry objective lens operating at 400 kV was used to analyse samples after specific reduction stages. In all cases images were recorded on negatives and afterwards digitized using a CCD camera; the gray scale was adapted to achieve reasonable contrast, but no filtering of images was performed. We did not observe a noticeable effect of the electron beam on the reduction kinetics, possibly because the bright and dark-field images were never recorded with a highly focused electron beam.

3. RESULTS AND DISCUSSION

3.1. Indentification of Mn_3O_4 and MnO precipitates

The reduction of Mn_3O_4 precipitates into MnO in an Ag matrix can be followed in-situ in a HRTEM using high resolution (HR) images or using conventional 2-beam images. The former has the advantage that atomic structure information is directly available. However, only one or a few neighbouring precipitates with typical size of 10 nm can be followed in this way and the statistics of the analysis will be rather poor. Further, during heating or heating/cooling cycles drift is substantial and it is rather difficult to keep track of a single precipitate in the HR mode. The 2-beam images do not suffer from these two disadvantages and, as will be shown below, they allow for a clear distinction between the different types of precipitates observed.

Strong-beam Ag200 and Ag220 dark-field images are shown in Figs 1(a and b), respectively, displaying the same sample area after reduction for 5 min at 500°C. The contrast in dark field appeared to be superior to that in bright field. The actual area shown in Fig. 1 is only about 4% of the total area captured in a single negative. Hence, it is clear that from a sequence of such observations the reduction of Mn_3O_4 into MnO can be followed with excellent statistics.

The precipitates in Fig. 1 can be identified on the basis of their Moiré pattern, resulting from the state of mismatch between the precipitate and the Ag matrix in combination with the imaging conditions, i.e. viewing direction and reflection used for imaging. In principle, three basic types of Moiré patterns can be recognized in the images. MnO precipitates give one type and Mn_3O_4 precipitates give two types depending on whether the a or the c axis of the tetragonal-spinel Mn_3O_4 is lying in the plane of projection. The presence of Moiré patterns indicates that the precipitates are not coherent with the matrix. In
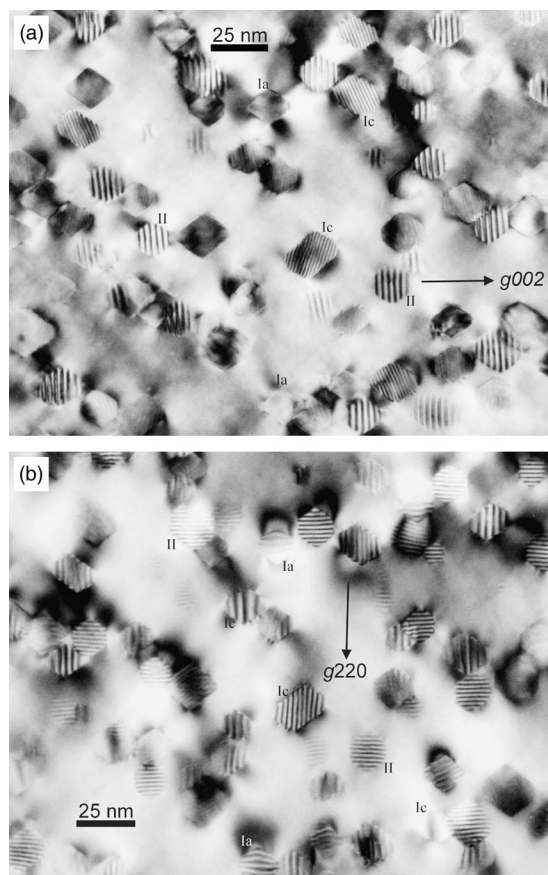
Fig. 1. Two-beam dark-field images showing the same area of an Ag matrix containing Mn_3O_4 precipitates after 5 min reduction at 500°C. A large fraction of Mn_3O_4 precipitates have been transformed into MnO. A few examples of MnO precipitates are indicated by the mark II and of Mn_3O_4 precipitates with an a axis (nearly) in the plane of projection are marked Ia and with the c axis (nearly) in the plane of projection Ic. After tilting about 6° out of the Ag<110] zone axis, (a) is recorded using the strongly excited Ag200 reflection and (b) using the Ag220 one.

references [28, 29, 31, 33, 34], much effort was devoted to demonstrate the presence of (localized) misfit dislocations at the precipitate–matrix interfaces and thus the semi-coherent nature of the interfaces. Most long-range stresses present for coherent precipitates vanish for semi-coherent ones.

MnO having the NaCl-type structure and the fcc Ag matrix exhibit a parallel topotaxy. Therefore the g-vectors of MnO and Ag are always parallel and the Moiré patterns observed are only of translational type, meaning that the Moiré fringes are perpendicular to the g-vectors used. Due to the mismatch of MnO ($a = 0.4444$ nm) and Ag ($a = 0.4089$ nm) the fringe spacing corresponds to 2.59 and 1.83 nm for using the 200 and 220 reflections, respectively. As examples, two MnO precipitates in Fig. 1 are indicated by the mark II. The observed Moiré fringes of Mn_3O_4 depend strongly on the combination of viewing direction and g-vector used. Since the dark-field images are taken by tilting the specimen 4–8° out of

the <110] Ag zone axis, the orientation of the Mn_3O_4 precipitates in the Ag matrix can be explained with reference to this zone axis. This zone axis is also used for HR imaging and details about the orientation of the Mn_3O_4 precipitates in the Ag matrix were already elaborated in [28], Section 3.2.

The following distinctions can be made:

(a) The two a axes and the c axis of Mn_3O_4 are parallel to the cube axes of Ag. The a axes do not give rise to a significant mismatch with the cube axes of Ag (only -0.4%), whereas along the c axis a mismatch of 15.4% occurs with respect to the Ag. Note that for the mismatch we compare the fcc Ag lattice with the fct oxygen-sublattice of Mn_3O_4 that can be described with half the lattice constants of Mn_3O_4. For viewing along Ag<110> one cube axis of Ag is in the plane of projection. Then the following two distinctions can be made:
(i) the Mn_3O_4 a axis is parallel to this Ag cube axis in the plane of projection.
(ii) the Mn_3O_4 c axis is parallel to this Ag cube axis in the plane of projection.
If in the case of (i) the Ag200 g-vector is used, no Moiré fringes are observed because no mismatch is present in that particular direction between Mn_3O_4 and Ag. If on the other hand the 220 g-vector is used, a translational Moiré with a spacing of 2.37 nm is observed due to the mismatch between the {220}Ag and {044}Mn_3O_4 plane spacing. (In fact the Ag220 and the $Mn_3O_4$044 g-vectors are only parallel in the projected view; they actually have a mutual rotation of 4.16° along the a axis/cube axis in the plane of projection. This does not influence the observed Moiré). If in the case of (ii) the Ag200 g-vector is used, a fine fringe spacing of 1.55 nm due to translational Moiré is observed reflecting the 15.4% mismatch with the Mn_3O_4 004 reflection. If on the other hand the Ag220 g-vector is used, no Moiré fringes will be observed since the g-vector is perpendicular to the mismatching c axis of Mn_3O_4.

(b) A deviation is now introduced with reference to the above starting configuration of case a. In the latter it was assumed that the principal axes of Mn_3O_4 were parallel to the cube axes of Ag. Then, all 8 {111} Mn_3O_4 and Ag planes (surrounding the octahedron) show a mutual tilt of 3.8° with as tilt-axis a <110> directions perpendicular to the c axis of Mn_3O_4. The Mn_3O_4 precipitates have an octahedral shape and are bounded by the 8 {111} planes. Now, instead of the tilt of 3.8° at all interfaces between {111} planes of Mn_3O_4 and Ag, most precipitates show a preference to rotate $\pm 3.8°$ along the <110> axes perpendicular to the Mn_3O_4 c axis to align the {111} planes of Mn_3O_4 and Ag parallel for one pair of facets of the octahedron. Then, for another pair of facets a tilt of 7.6° will occur and for the remaining two pairs of facets a

combined tilt and twist will occur between the {111} of Mn_3O_4 and Ag. Although a preference exists for the rotation of 3.8°, all rotations between 0 and ±3.8° can be observed in practice [28]. This rotation does not significantly affect the observed Moiré patterns described in case a–(i) above, since the rotation axis is inclined. In Fig. 1 two examples of Mn_3O_4 precipitates with the a axis in the plane of projection are marked by Ia. On the other hand, the Moiré patterns described under a–(ii) have a large probability to be changed significantly. This change occurs if the rotation axis is parallel to the viewing direction and the probability for this is 50%; the other 50% occurs if the Ag<110] direction lying in the plane of projection is the rotation axis. Particularly using the Ag220 reflection, see Fig. 1(b), the influence of the rotation can be observed and analysed distinctly. In a–(ii) no Moiré pattern would be observable. Due to a rotation around the viewing direction a rotational Moiré, i.e. with the fringes parallel to the g-vector, will arise and the distance between the fringes is a direct measure of the rotation angle. For an angle of 3.8° the fringe spacing is 2.18 nm. Using the Ag002 reflection, see Fig. 1(a), the influence of the rotation is less distinct. It rotates the fine fringes slightly off from being perpendicular to the g-vector; the sense of rotation, clock or counter-clockwise can be observed in Fig. 1(a). For a rotation of 3.8° the translational Moiré with a fringe spacing of 1.55 nm will become a general Moiré with a spacing of 1.41 nm. In Fig. 1(b) the rotational Moiré is always parallel to the g-vector. In Fig. 1 some of the Mn_3O_4 precipitates with the c axis in the plane of projection are marked by Ic.

The dark-field images using the Ag220 reflections are most characteristic and sufficient for following the Mn_3O_4 reduction in-situ and were used during the rest of the research. A remarkable feature of the Mn_3O_4 precipitates with the a axis in the plane of projection, i.e. case a–(i) or b–(i) is the strain field in the matrix around the precipitates. Particularly using the Ag220 reflection, the curved strain fields near the blunt corners of the precipitates in the Ag and the curved Moiré fringes (reflecting an inhomogeneous state of mismatch between the Ag and Mn_3O_4 throughout the projected area of the precipitates) can be observed nicely. Apparently the misfit dislocations present cannot cancel all long-range stresses. This is not surprising since only the large mismatch due to the Mn_3O_4 c axis (15.4%) is relieved by misfit dislocations and the small mismatch due to the a axes (−0.4%) probably causes the coherency strains.

The preference of precipitates to rotate 3.8° to align the {111} planes of Ag and Mn_3O_4 parallel for one pair of facets as described above under case b can be understood on the basis of the interface energy. One pair of facets with {111} planes aligned parallel plus one pair with a tilt of 7.6° corresponds to a lower interface energy than two pairs of facets with a tilt of 3.8°, because of the convex shape of the cusp in the interface energy as a function of the tilt angle.

3.2. Reduction rate

The kinetics of the reduction of Mn_3O_4 precipitates into MnO was studied at 400, 500, 600 and 700°C nominal temperature. The 2-beam dark-field images employing the Ag220 reflection as explained in the previous section were used to monitor the rate of reduction. All precipitates in a certain area (of about 150×150 nm^2) close to the edge with the hole in the Ag foil were analyzed. Their total number at the start of the reduction corresponded to 124 at 400°C, 72 at 500°C and 154 at 600°C. The results of the 400 and 600°C series are shown in Figs 2(a and b), respectively. The results of the 500°C series resembles very closely to the 400°C one, and at 700°C the transformation took place so fast that within 30 s all observable Mn_3O_4 precipitates were already turned into MnO.

A characteristic feature of the 400 and 500°C results is that a plateau is reached where a certain fraction of precipitates, typically of the order of 50% is transformed into MnO whereas the other 50% does not to transform. Although this plateau is reached already after about 5 min, the next 2 h of annealing does not lead to any significant increase in the fraction of reduced precipitates. Apparently, for these precipitates a barrier of activation energy is present which cannot be overcome at these temperatures. On the other hand, at 700°C no barrier seems to be present. The transformation at 600°C is an important intermediate case; it first shows a rapid transformation of about 50% of the precipitates and then a slight retardation of the reduction rate occurs in which a significant fraction of mixed Mn_3O_4/MnO precipitates can be observed. Subsequently an increase in the reduction rate is observed which finally results in 100% transformed precipitates. At temperatures other than 600°C individual precipitates transform so fast that the Mn_3O_4/MnO intermediate state is not observed. Apparently, the second 50% of precipitates have much more difficulty to transform than the first 50% explaining that the mixed precipitates are formed at the onset of the transformation of the second 50%.

An important observation is that the level of the plateau reached at 400 and 500°C clearly depends on the thickness of the Ag foil in which the precipitates are embedded. Close to the edge of the hole of the wedge-shaped sample a larger fraction of finally transformed precipitates is observed than at larger distances from the hole. At first sight an explanation based on kinetics might be given, i.e. in a thicker area more time is needed before the oxygen can diffuse out of the Ag foil. However, as already stated above this explanation does not hold because on prolonged heating the fraction of precipitates that transform does not increase. As we will explain in the next section
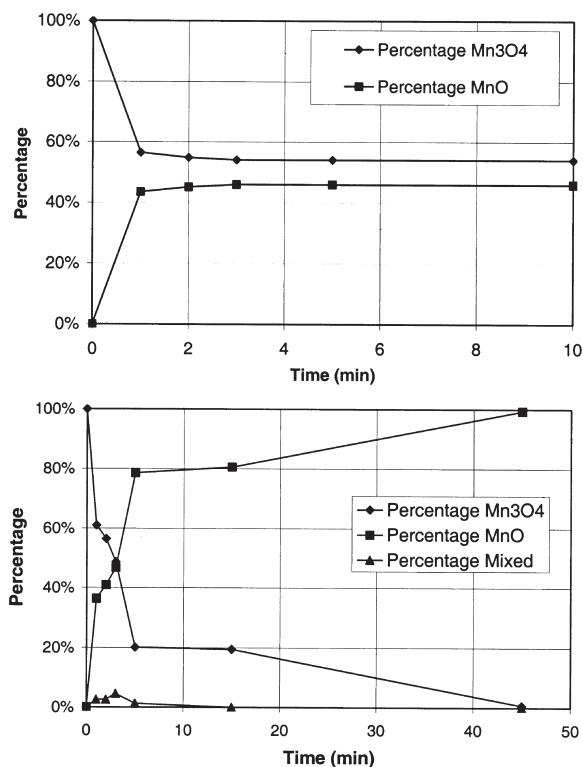
Fig. 2. Fraction of Mn_3O_4 and MnO precipitates as a function of annealing time in reducing atmosphere at 400°C (a) and 600°C (b).

the observed reduction kinetics in the range from 400 to 700°C can be explained rather well by the influence of the volume reduction of the precipitates upon oxide reduction in conjunction with the Ag self-diffusion transporting Ag atoms from the sample surface to the interior where the volume reduction operates.

3.3. Lattice expansion, volume reduction and shape change

An important aspect of the transformation of Mn_3O_4 precipitates into MnO is the accompanied volume reduction. The a axes of Mn_3O_4 are 0.814 nm and the c axis is 9.42 nm [35]. The oxygen sublattice in Mn_3O_4 is fct with a axes of 0.407 and the c axis of 0.471 nm. Since during the Mn_3O_4 to MnO transformation it is inevitable that the oxygen sublattice is maintained (only the tetragonal distortion disappears) and that the Mn cations are redistributed over the interstices constituted by the O-sublattice, the fct O-sublattice of Mn_3O_4 can be directly compared with the fcc O-sublattice of MnO having a lattice constant of 0.4444 nm. So, the a axes of Mn_3O_4 will expand by 9.2% and the c axis will contract by 5.6%. Per unit cell of MnO a volume expansion of 12.5% occurs compared to the unit cell of the fct O-sublattice of Mn_3O_4. However, the reduction of Mn_3O_4 into MnO is achieved by using Ti as an oxygen getter and approximately a quarter of the original oxygen anions will be removed and Mn_3O_3 remains. Therefore, although a lattice expansion occurs, the total volume

of an Mn_3O_4 precipitate will be reduced by 15.6% during the reduction process.

The driving force for the reduction of Mn_3O_4 precipitates into MnO is the change in Gibbs-free energy for the reaction where Ti+Mn_3O_4 changes into Ti-oxide(e.g. TiO_2)+MnO. The Gibbs-free energy is composed of contributions of the bulk phases and incorporates strain and interfacial energy. In particular, the Ag/Mn_3O_4, Ag/MnO and Ti/TiO_2 interfaces are of importance here. During the transformation within the precipitates Mn_3O_4/MnO interfaces are formed which contribute to the activation energy of the reduction process. The volume reduction of the precipitates may either induce large strains if the compatibility of the precipitate/matrix interface is maintained or in the case that voids between the precipitate and matrix are generated interfacial energy terms have to be added (precipitate/matrix interface splits into precipitate/vacuum+vacuum/matrix interfaces). According to Fig. 1 and for the large numbers of precipitates analysed the volume reduction never led to the formation of voids at the precipitate/matrix interface in the Mn_3O_4/Ag system. (In the Mn_3O_4/Pd system where the oxide precipitates are larger by a factor of about 10 than in the Mn_3O_4/Ag system [31] and where in TEM foils the oxide precipitates are no longer embedded within the metal matrix, holes were generated at Pd/Mn_3O_4 interfaces upon reduction. Also, the interfaces roughened considerably due to local diffusion of Pd across the interface to compen-

sate for the volume reduction of the oxide precipitate.) Consequently, during the Mn_3O_4 to MnO transformation strains develop within the Ag matrix which further oppose the transformation process and even may prevent it. This holds for the 50% of non-transforming precipitates at 400 and 500°C. Despite the volume reduction, strain fields around the transformed MnO precipitates are almost never observed and apparently a strain–relaxation mechanism is operative. Based on the observations, the conclusion can be drawn that MnO cannot develop without strain relaxation.

The first step in the reduction is the out-diffusion of oxygen and the coupled in-diffusion of vacancies with respect to the Ag foil. The in-diffusion of vacancies associated with the volume reduction can be counteracted by the out-diffusion of vacancies and the coupled in-diffusion of silver atoms from the sample surface to the location where the volume reduction occurs. Hence, the in-diffusion of Ag acts as the strain relaxation mechanism mentioned above. In this context the inter- and self-diffusion coefficients of oxygen and Ag in the Ag matrix respectively are of importance. The diffusion of O in Ag is extremely fast [36], i.e. about four orders of magnitude faster than the diffusion of Mn [37]. Actually, it is one of the requirements that makes the internal oxidation of manganese inside the Ag matrix possible anyway. The Mn diffusion in Ag [38] is rather comparable to the Ag self-diffusion [39]. If the oxygen diffusion through the Ag is the rate-limiting step of the transformation, it may proceed extremely fast. On the other hand, if the self-diffusion of Ag is rate determining, the transformation will be much slower. At 400°C the average distance, i.e. $\sqrt{Dt}$, Ag atoms can diffuse within 1000 s is about 14 nm. At 700°C this distance has increased to 2.4 μm. Because the actual temperatures at the thin edge in the TEM samples are lower than the nominal ones the diffusion distances will be somewhat less.

At 400 and 500°C the Ag self-diffusion compared to the O diffusion in Ag is so slow that the volume reduction and the build up of strain cannot be counteracted effectively and the volume reduction prevents the Mn_3O_4 to MnO reduction. Only the precipitates that are close enough to the sample surface can relax their strains and are able to transform. This explains the dependence of the fraction of precipitates that can transform at 400 and 500°C on the local thickness of the Ag foil (i.e. on the distance to the edge of the hole in the sample). On the other hand, at 700°C the Ag self-diffusion is fast enough to prevent any noticeable effect of build up of strain due to the volume reduction and therefore the transformation can occur without any sign that an activation barrier has to be overcome. The mixed precipitates at 600°C denote precipitates which during transformation build up strain preventing further transformation. After a certain incubation time in which the Ag self-diffusion relaxes the strains the transformation can continue.

Although it is shown here in detail for the Mn_3O_4 to MnO transformation only, it is quite obvious that in general a volume change accompanying a phase transformation in inclusions will have a crucial effect on the transformation kinetics. In particular because the Ag matrix is rather compliant and deforms plastically, this study exemplifies a system for which the volume change is accommodated relatively easily. Hence, in most systems the volume change will play an even more predominant role than in the present one.

The volume reduction is accompanied with a change of the shape of the Mn_3O_4 precipitates from an octahedral one with only small {200} and (002) facets to a nearly cuboctahedral one of the MnO particles with wide facets. If the whole volume change starting from complete octahedrons is realized by the formation of the {200} facets, the relative truncation will be 38.5% along the former a axes and 467.8% along the former c axis. The relative truncation is defined by the width of the {200} facets in a {110} cross section divided by the width of the particle at the equator. The experimental values of the truncation range between 30 and 45% with an average of approximately 37%. Since the original Mn_3O_4 precipitates are elongated along the c axes but the final MnO precipitates do not show preferred orientations of the truncation, the particles must have shrunk particularly in their c directions.

Of course, the ratio of the {200} to {111} MnO/Ag facet lengths is in case of an equilibrium shape of the MnO precipitate directly proportional to the ratio of their interfacial energies. So, although most of the volume reduction appears to be absorbed in the increased truncation, this is only possible because the {200} MnO/Ag interface becomes more stable with respect to the {111} one. Such an increase of the size of the {200} relative to the {111} facets upon reduction is expected in the light of the results presented in [40] for Cu/MgO interfaces. Also, in our reduction experiment the sample will be more or less in equilibrium with a reduced oxygen partial pressure. In the starting condition this pressure corresponds approximately to the ambient pressure since the internal oxidation is performed in air and in the final condition it will approach the dissociation pressure of Ti-oxide (e.g. TiO_2). In the starting condition the terminating {111} planes of Mn_3O_4 at the interface are a polar planes of oxygen atoms only [41–45]. Upon sufficient reduction the terminating planes will be composed of Mn cations (or they have at least a much reduced oxygen occupancy) [41, 45]. Instead, the non-polar {200} planes remain on all conditions composed of 50% anions and 50% cations. Thus, a qualitative explanation for the reduced stability of {111} plane with respect to {200} one is that the fraction of direct nearest-neighbour oxygen–metal bonds across the interface strongly decreases for {111} (because they become replaced by cation–metal

bonds) whereas this fraction remains the same for {200}.

3.4. Mixed precipitates of both Mn_3O_4 and MnO

As explained in Section 3.2, mixed precipitates lying away from the free surface were observed only during the first 10 min of reduction at 600°C. As explained in Section 3.1, the 2-beam dark-field images employing the Ag220 reflection revealed the presence of mixed precipitates particularly for the Mn_3O_4 precipitates with their c axis in the plane of projection (type Ic). These precipitates exhibit a rotational Moiré pattern with the fringes parallel to the g-vector. The newly formed MnO precipitates (type II) on the other hand will show translational Moiré with the fringes perpendicular to the g-vector. Thus, these mixed precipitates can easily be distinguished, since they show two parts with mutually orthogonal fringes. This does not hold for the Mn_3O_4 precipitates with their a axis in the plane of projection (type Ia). Then, in both parts the fringes are perpendicular to the g-vector and only their spacings differs.

The 2-beam dark-field images recorded at a magnification of 80,000 times are well suited to analyse a large number of precipitates simultaneously, but not to determine accurately enough the atomic plane forming the Mn_3O_4/MnO interface within the mixed precipitates. Still, the detected interfaces appeared to make an angle of about 45° and appeared to be approximately parallel to one of the {111} facets of the precipitate. High-resolution images taken at a microscope magnification of 500,000 times are much better suited for detecting the interface plane. To this end an Ag/Mn_3O_4 sample was heated 5 min at 600°C and afterwards analysed at room temperature with high-resolution TEM. In order to observe the Moiré fringes corresponding to the 2-beam dark-field images obtained with the Ag220 g-vector, many-beam images were recorded by tilting the specimen by about 4° out of the Ag<110] zone axis such that a strong Ag220 beam was included. Two examples of mixed precipitates observed under these conditions are shown in Figs 3 and 4. Figure 5 presents a mixed precipitate observed "exactly" in the Ag<110] zone axis. These three images clearly indicate that the Mn_3O_4/MnO interface within the precipitates are preferentially oriented parallel to {111} of Ag, Mn_3O_4 and MnO, although it remains difficult to locate the interface on the atomic scale.

The following explanation(s) can be given for the observed preferred orientation of the Mn_3O_4/MnO interface within the precipitates during transformation. In the final state the MnO precipitates show a parallel topotaxy with the Ag matrix; all directions and planes in MnO and Ag are parallel. On the other hand, the initial Mn_3O_4 precipitates can only have one or two planes and directions parallel with those of the Ag matrix, with a preference for aligning {111} of Mn_3O_4 and Ag parallel for one pair of facets. Then, for instance the c axis of Mn_3O_4 makes an angle of
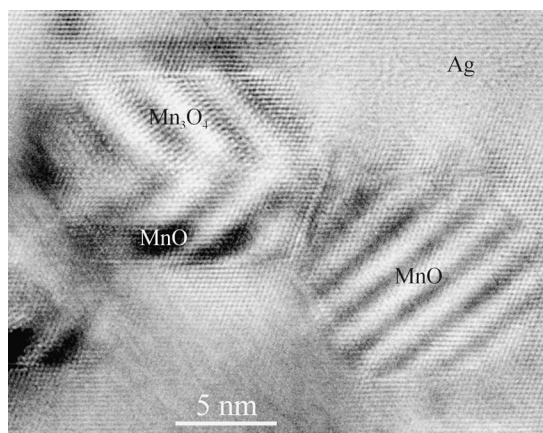

Fig. 3. HRTEM image of a mixed Mn_3O_4/MnO precipitate recorded by tilting the specimen 6° out of the Ag<110] zone axis such that a strongly excited Ag220 reflection is included in the many-beam image. The Mn_3O_4 and MnO parts of the precipitate can be distinguished easily on the basis of the mutual orthogonal Moiré fringes. The Mn_3O_4 part has the c axis nearly in the plane of projection.
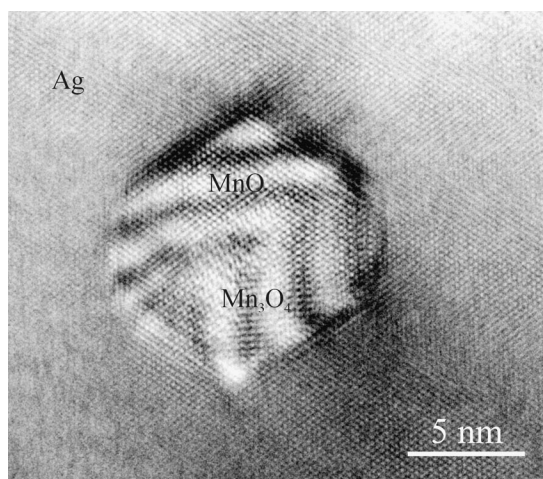

Fig. 4. HRTEM image of a mixed Mn_3O_4/MnO precipitate recorded by tilting the specimen 3° out of the Ag<110] zone axis such that a strongly excited Ag220 reflection is included in the many-beam image. The Mn_3O_4 and MnO parts of the precipitate can be distinguished on the basis of the mutual orthogonal Moiré fringes. The Mn_3O_4 part has the c axis nearly in the plane of projection.

3.8° with the nearest cube-axis of Ag. Now, the energetically most favourable state for the forming MnO is probably that which is parallel to both the Ag and Mn_3O_4 and thus should proceed with an interface oriented parallel to e.g. the {111}face that is parallel for Ag and Mn_3O_4. In addition to this argument based on parallelism another interesting aspect is the presence of an invariant line for the Mn_3O_4 and MnO lattices [46, 47]. Such an invariant line is possible because the Bain-strain lattice correspondence relating the oxygen sublattices of Mn_3O_4 and MnO has mixed signs of the strains. The invariant line corresponds to any direction on the cone making an angle of 37.1° with
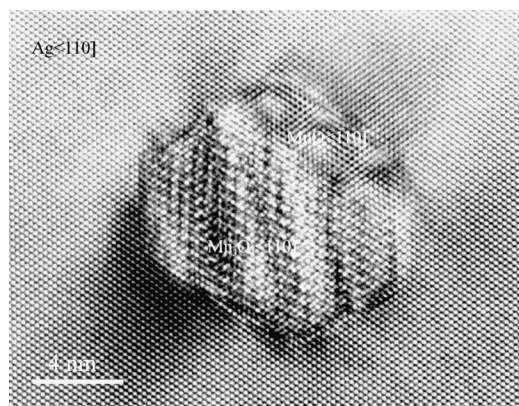
Fig. 5. HRTEM image of a mixed Mn_3O_4/MnO precipitate recorded (as exact as possible) in the Ag<110] zone axis. The Mn_3O_4 part has the c axis in the plane of projection.

the c axis of Mn_3O_4. After the Bain distortion these invariant-line directions constitute a cone making an angle of 41.2° with the "c axis" of MnO and thus if MnO and Mn_3O_4 lattices are related by an invariant line they are related by a rotation of 4.1° around the [hk0] perpendicular to the invariant-line direction. If a {111} plane of MnO becomes parallel to a {111} plane of Mn_3O_4, the rotation is 3.8°, which is already near to the 4.1° needed for the invariant line. Moreover, the {111} plane makes an angle of 35.3° and 31.4° with the c axis of MnO and Mn_3O_4 respectively, which is not far off (within 6° off) the angles needed for an interface plane containing an invariant line. Note that for the Mn_3O_4{111} plane that is tilted by 7.60 with respect to the Ag{111} plane, the sense of rotation is wrong, i.e. −3.8° when ±4.1° is needed for the invariant line. Indeed, the Mn_3O_4/MnO interface is never observed parallel to this tilted interface.

As described in out previous paper [30] the same arguments apply to the reverse MnO to Mn_3O_4 transformation. There, it was argued that the plane containing the invariant line exactly connects planes in the Mn_3O_4 and MnO structures with different cation occupancies, different polarity, etc., and thus introduces a defect structure at the interface. This is not the case for {111} planes because in both Mn_3O_4 and MnO they can consist of close-packed oxygen planes. So, it is likely that the interfacial energy increase due the small deviation from the plane containing the invariant line exactly is balanced by the decrease due to the further defect-free nature of {111} planes with respect to both Mn_3O_4 and MnO.

3.5. Ostwald ripening

In the sequence of the 2-beam dark-field images (Section 3.2) also the growth of MnO precipitates after reduction is observed. In most cases Ostwald ripening took place, although some clustering was observed as well. At clustering, the precipitates approach each other, whereas at Ostwald ripening the bigger precipitate remains at its original location. In

Figs 6(a and b) an example of clustering and in Figs 7(a and b) an example of Ostwald ripening is shown. Both pairs were recorded after 1 and 45 min at 600°C, respectively. At 400°C no signs of Ostwald ripening (or clustering) were observed during the 3 h of reduction monitored. At 500°C Ostwald ripening was observed after 2 h reduction and at 600°C already after 3 min. Note that at 500°C, although only a fraction of Mn_3O_4 precipitates can transform, still this limited MnO fraction can show Ostwald ripening. The observations indicate that for increasing temperature Ostwald ripening occurs sooner after the start of the reduction. As already discussed in Section 3.3, the O diffusion in Ag is about four orders of magnitude faster than that of Mn in Ag. Thus, for Ostwald ripening the rate-limiting factor is the transport of Mn from one precipitate to the other. Reduction if not hampered by the volume decrease is determined by the O diffusion. Thus, the observed incubation time between the onset of the reduction and the onset of Ostwald ripening is probably a reflection of the difference in the rates of O and Mn diffusion in the Ag matrix.

4. CONCLUSIONS

- In the present work, a convenient method is demonstrated for monitoring phase transformations in a large number of inclusions simultaneously by in-situ TEM. The method employs 2-beam dark-field images giving distinct Moiré patterns for the different types of precipitates. It is applied here to the Mn_3O_4 to MnO transformation for nano-sized oxide precipitates in a silver matrix.
- It is shown that volume changes accompanying the phase transformation will in general have a controlling influence on the transformation kinetics. For the Mn_3O_4 to MnO transformation the volume reduction of the precipitates may even prevent the transformation. It occurs only if the strains due to the volume reduction are relaxed and this is possible: (i) if the precipitates are close enough to a free surface of the Ag foil or (ii) if the Ag self-diffusion is fast enough to compensate for the volume reduction by transporting Ag atoms from the surface to the interior where the volume reduction occurs. At 400 and 500°C, only mechanism (i) is active, at 600°C mechanism (ii) starts slightly later than mechanism (i) and at 700°C mechanism (ii) becomes so fast that it cannot be distinguished any more from (i).
- Shape changes of the oxide precipitates in a metal matrix upon reduction also reflect the changed stability of the various facets due to the equilibration in a reduced oxygen partial pressure. The volume reduction accompanying the Mn_3O_4 to MnO transformation appeared to be largely absorbed in the increased truncation of the octahedrons by {200} facets. This increased truncation is a consequence of the reduced oxygen partial
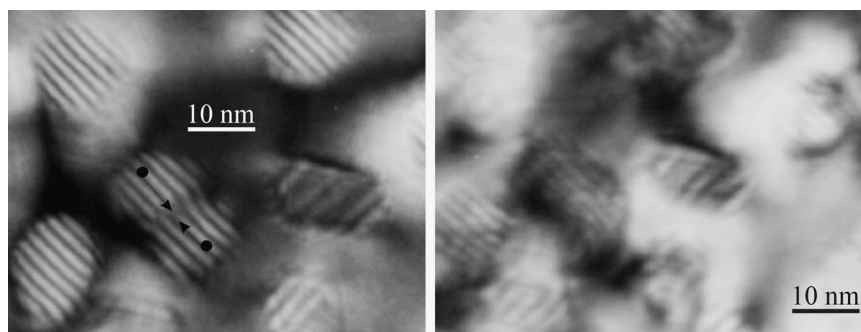
Fig. 6. Two-beam dark-field images employing the strong Ag220 beam after 1 min reduction (a) and after 45 min reduction (b) at 600°C. Comparison of the two images shows that clustering of two neighboring MnO precipitates has occurred. Clustering is an usual phenomenon. Generally Ostwald ripening occurs (see Fig. 7).
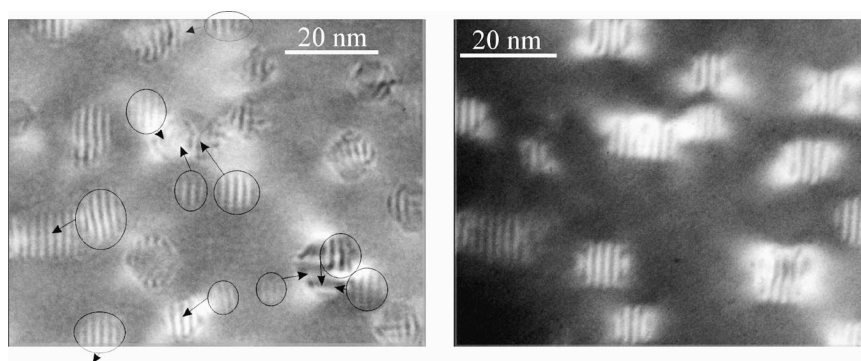

Fig. 7. Two-beam dark-field images employing the strong Ag220 beam after 1 min reduction (a) and after 45 min reduction (b) at 600°C. Comparison of the two images shows that Ostwald ripening of neighboring MnO precipitates has occurred. In (a) the arrows give a tentative indication of which bigger precipitates swallow the smaller ones.

pressure which increases the energy of the {111} facets compared to the {200} ones.

- Mixed Mn_3O_4/MnO precipitates were only observed at 600°C in a short time interval denoting the initial stage in which the above mechanism (ii) becomes active after mechanism (i). The Mn_3O_4/MnO interface passing through the precipitate upon reduction tends to orient parallel to that {111} plane of Mn_3O_4 and Ag which is aligned parallel for the one pair of facets of the precipitate.

- Ostwald ripening of the MnO precipitates is observed after reduction. The incubation time between the start of the reduction and the start of the Ostwald ripening reflects the difference in the diffusion coefficient of oxygen and Mn in an Ag matrix; oxygen diffusion being much faster than Mn diffusion.

REFERENCES

1. Dahmen, U., Xiao, S. Q., Paciornik, S., Johnson, E. and Johansen, A., *Phys. Rev. Lett.*, 1997, **78**, 471.
2. vom Felde, A., Fink, J., Müller-Heinzerling, Th., Pfüger, J., Scheerer, B., Linker, G. and Kaletta, D., *Phys. Rev. Lett.*, 1984, **53**, 922.
3. Templier, C., Jaouen, C., Reviere, J. P., Delafond, J. and Grilhe, J., *C.R. Acad. Sci. Ser. 2*, 1984, **299**, 613.
4. Porterling, D. A. and Easterling, K. E., *Phase Transformations in Metals and Alloys*. Van Nostrand Reinhold, New York, 1980.
5. Takagi, M., *J. Phys. Soc. Jpn*, 1954, **9**, 359.
6. Borel, J., *Surf. Sci.*, 1981, **106**, 1.
7. Goldstein, A. N., Echer, C. M. and Alivisatos, A. P., *Science*, 1992, **256**, 1425.
8. Ben David, T., Lereah, Y., Deutscher, G., Kofman, R. and Cheyssac, P., *Phil. Mag.*, 1995, **A 71**, 1135–1143.
9. Moore, K. I., Chattopadhyay, K. and Cantor, B., *Proc. Roy. Soc. Lond.*, 1987, **A 414**, 499.
10. Saka, H., Nishikawa, Y. and Imura, T., *Phil. Mag.*, 1988, **A 57**, 895.
11. Grabaek, L., Bohr, J., Andersen, H. H., Johansen, A., Johnson, E., Sarholt-Kristensen, L. and Robinson, I. K., *Phys. Rev. B.*, 1992, **45**, 2628–2637.
12. Andersen, H. H. and Johnson, E., *Nucl. Instr. Meth.*, 1995, **B 106**, 480.

13. Goswami, R., Chattopadhyay, K. and Ryder, P. L., *Acta. Mater.*, 1998, **46**, 4257.
14. Hagege, S., *Interface Sci.*, 1999, **7**, 85.
15. Rühle, M., Kraus, B., Strecker, A. and Waidelich, D., in, *Science and Technology of Zirconia II, Advances in Ceramics*, ed. N. Clausen, M. Rühle and A. H. Heuer, Vol. 12. The American Ceramic Society, Columbus, OH, 1984, p. 256.
16. Lee, R. R. and Heuer, A. H., *J. Am. Ceram. Soc.*, 1988, **71**, 701.
17. Rühle, M., Ma, L. T., Wunderlich, W. and Evans, A. G., *Physica B*, 1988, **150**, 86.
18. McCartney, M. R. and Rühle, M., *Acta. Metall.*, 1989, **37**, 1859.
19. Lin, G. Y., Lei, T. C. and Zhou, Y., *Ceram. Intern.*, 1998, **24**, 307.
20. Schofield, M. A., Aita, C. R., Rice, P. M. and Gajdardziska-Josifovska, M., *Thin Sol. Films*, 1998, **326**, 117.
21. Evans, A. G. and Cannon, R. M., *Acta. Metall.*, 1986, **34**, 761.
22. Green, D. J., Hannink, R. H. J. and Swain, M. V., *Transformation Toughening Ceramics*. CRC, Boca Raton, FL, 1989.
23. Rühle, M., Claussen, N. and Heuer, A. H., *J. Am. Ceram. Soc.*, 1986, **69**, 195.
24. Rühle, M., Evans, A. G., McMeeking, R. M. and Hutchinson, J. W., *Acta. Metall.*, 1987, **35**, 2701.
25. van Tendeloo, G., van Landuyt, J. and Amelinckx, S., *Phys. Stat. Solid. (a)*, 1976, **33**, 723.
26. Yamamoto, N., Tsuda, K. and Yagi, K., *J. Phys. Soc. Jpn*, 1988, **57**, 2559.
27. Smith, D. J., *Nato ASI Ser.*, 1988, **B 191**, 43.
28. Kooi, B. J., Groen, H. B. and De Hosson, J. Th. M., *Acta Mater.*, 1997, **45**, 3587.
29. Kooi, B. J., Groen, H. B. and De Hosson, J. Th. M., *Acta Mater.*, 1998, **46**, 111.
30. Kooi, B. J. and De Hosson, J. Th. M., *Acta Mater.*, 1998, **46**, 1909.
31. Kooi, B. J. and De Hosson, J. Th. M., *Acta Mater.* 2000, **48**, in press.
32. Kooi, B. J., Westers, A. R., Vreeling, J. A., van Agterveld, D. T. L. and De Hosson, J. Th. M., *Mat. Sci. Forum*, 1999, **294–296**, 255.
33. De Hosson, J. Th. M., Groen, H. B., Kooi, B. J. and Vitek, V., *Acta Mater.*, 1999, **47**, 4077.
34. Groen, H.B., Kooi, B.J., Vellinga, W.P. and De Hosson, J.Th.M., *Phil. Mag. A* **79**, 2083.
35. Wyckoff, R. W. G., *Crystal Structures*, 2nd edn. Interscience Publishers, New York, 1963.
36. Diffusion Data 3, 1969, 12.
37. Meijering, J. L., *Adv. Mater. Res.*, 1971, **5**, 1.
38. Diffusion and Defect Data 21 1980, 1.
39. Mrowec, S., *Defects and Diffusion in Solids, an Introduction, Materials Science Monographs 5*, Elsevier, Amsterdam, 1980.
40. Backhaus-Ricoult, M. and Laurent, S., *Mater. Sci. Forum*, 1999, 294–296, 173.
41. Mader, W., *Z. Metallkd.*, 1992, **83**, 7.
42. Jang, H., Seidman, D. N. and Merkle, K. L., *Interface Sci.*, 1993, **1**, 61.
43. Muller, D. A., Shaskov, D. A., Benedek, R., Yang, L. H., Silcox, J. and Seidman, D. N., *Phys. Rev. Lett.*, 1998, **80**, 4741.
44. Shashkov, D. A., Muller, D. A. and Seidman, D. N., *Acta. Mater.*, 1999, **47**, 3953–3963.
45. Laurent, S., Imhoff, D., Colliex, C., Htch, M. J., Devaud, J., Hagege, S. and Backhaus-Ricoult, M., *Mat. Sci. Forum*, 1999, 294–296, 325.
46. Dahmen, U., *Acta Metall.*, 1982, **30**, 63.
47. Dahmen, U. and Westmacott, K. H., *Acta Metall.*, 1986, **34**, 475.